Electronic Supplementary Information

Native defects determine phase-dependent photoluminescence behavior of Eu^{2+} and Eu^{3+} in In_2O_3 nanocrystals

Vahid Ghodsi, Arunasish Layek, Manu Hegde, Baran Yildirim and Pavle V. Radovanovic*

Department of Chemistry, University of Waterloo, 200 University Avenue West, Waterloo, Ontario N2L 3G1, Canada

* To whom correspondence should be addressed. E-mail: pavler@uwaterloo.ca

I. EXPERIMENTAL AND THEORETICAL DETAILS

Materials. All reagents and solvents are commercially available, and were used as received. Indium acetylacetonate ($In(acac)_3$; 98%) and europium chloride ($EuCl_3$; 99.9%) were purchased from STREM Chemicals. Oleylamine (70%), tri-n-octylphosphine oxide (TOPO; 90%), and hexane (98.5%) were purchased from Sigma-Aldrich Corporation. Ethanol was obtained from Fisher Chemicals.

Synthesis of Eu-Doped Indium Oxide Nanocrystals. The synthesis of colloidal In_2O_3 NCs was performed in oleylamine (OA) as a coordinating solvent and reducing agent. In a typical synthesis, in a 100 mL round bottom flask, 1.0 g of $In(acac)_3$ and 10 g of OA were combined with different amounts of $EuCl_3$ (0.5−15 mol % relative to In). The solution was magnetically stirred and heated to desired temperature (200-300 ^oC), and refluxed over the course of 1 h. The resulting suspension was cooled to room temperature, precipitated, and washed three times with ethanol. After the final washing, TOPO was added to the precipitated NCs in an approximately volume-equivalent amount. The NCs were then heated and stirred in TOPO in a 90 ^oC oil bath for 1 h, and

subsequently precipitated and washed with ethanol. The TOPO treatment was repeated two more times, and TOPO-capped NCs were subsequently dispersed in hexane.

Nanocrystal Characterization. Nanocrystal size and structure were characterized by transmission electron microscopy (TEM) and powder X-ray diffraction (XRD). XRD patterns were recorded with INEL powder diffractometer having a Cu Kα radiation source and a position-sensitive detector. TEM imaging and energy dispersive X-ray spectroscopy (EDX) elemental analysis were performed with a JEOL-2010F microscope operating at 200 kV. The dilute suspensions of colloidal NCs in toluene were drop casted on TEM copper grids with lacey formvar/carbon support films purchased from Ted Pella, Inc. The europium doping concentrations determined by EDX were in good agreement with the concentrations determined by inductively coupled plasma atomic emission spectrometry (ICP-AES), and are defined as a percent of substituted In^{3+} ions.

Absorption and PL Measurements. All spectroscopic measurements were performed at room temperature. The absorption spectra of colloidal NCs were collected with a Varian Cary 5000 UV−vis-NIR spectrophotometer, in a 1 cm path length quartz cuvette. Steady-state PL excitation and emission spectra of colloidal NCs were measured with a Varian Cary Eclipse spectrometer, using standard quartz fluorescence cuvettes. For the direct comparison of PL intensities, the concentrations of colloidal suspensions of NCs were adjusted to exhibit the band gap absorbance of 1.0 at 300 nm and 270 nm for bcc-In_2O_3 and rh-In_2O_3 NCs, respectively. For Eu^{3+} PL emission measurements, the samples were excited at the excitation band maxima for bcc-In_2O_3 and rh-In_2O_3 NCs. The PL spectra of Eu^{2+} were measured upon excitation at 300 nm. For PL excitation measurements, the emission was monitored at the maximum of the Eu^{2+} 4f−5d transition band (402 nm) or at

the maximum of the Eu^{3+} $^5D_0 \rightarrow {}^7F_2$ peak (614 nm). Emission and excitation spectra for Eu^{3+} dopants were recorded in the phosphorescence mode (with 0.1 ms delay time and 5 ms gate time), using a Xenon flash lamp as the excitation source. High-resolution PL spectra were measured with a Renishaw 1000 spectrometer. For these measurements the NCs were deposited on a silicon substrate and excited at ca. 260 nm using frequency-tripled Millenia-pumped Tsunami laser (SpectraPhysics).

Time-resolved PL Measurements. Time-resolved measurements of Eu^{2+} dopant and defect-based DAP emissions were performed by time-correlated single photon counting (TCSPC) method with a Horiba Jobin Yvon IBH Ltd. spectrometer. A 250 nm NanoLED (IBH Ltd.) was used as the excitation source, and the signal was monitored at the corresponding emission band maxima. The instrument response function (IRF) was recorded by detecting the scattered excitation using a Ludox solution (Sigma Aldrich), and the data were fit with exponential function. Time decay of Eu^{3+} was measured with a Varian Cary Eclipse fluorescence spectrometer. In a typical experiment, the delay was set to 0.01 ms and the excitation wavelength was 230 nm. The signals were detected at the maximum of the $^5D_0 \rightarrow {}^7F_2$ peak (614 nm).

X-ray Absorption Spectroscopy Measurements. The Eu M-edge X-ray absorption spectroscopy measurements were performed at the Spherical Grating Monochromator (SGM) beamline 11ID-1 at the Canadian Light Source. Eu-doped In_2O_3 NC samples in the powder form were deposited on the carbon tape attached to the custom made copper sample holder. The sample stage was inserted in ultra-high vacuum (UHV) X-ray chamber using a load-lock procedure. The signal was detected by both total electron yield (TEY) and total fluorescence yield (TFY) using channel plate detectors.

Multiplet Structure Calculations. The ratio of Eu^{2+}/Eu^{3+} in Eu-doped In_2O_3 NC samples was determined by comparison of measured Eu M-edge X-ray absorption spectra (XAS) with the linear combinations of the theoretical Eu^{2+} and Eu^{3+} spectra, which were reproduced within the atomic multiplet calculations.[S1] The spin-orbit coupling term was included in the calculations. Assuming dipole selection rule $\Delta J = 0, \pm 1$ in the calculation reduces the total number of final states and reproduces simulated $M_{4,5}$-edge spectra. The simulated relative intensities corresponding to transitions in Eu^{2+} ($3d^{10}4f^7$ ($^8S_{7/2}$)$\rightarrow$ $3d^9 4f^8$ (^7F)) and Eu^{3+} ($3d^{10}4f^6$ (^7F) $\rightarrow$ $3d^9 4f^7$ (^8S)) are shown in Figure 3a (vertical lines). The Slater integral parameters (F^k) for the Eu^{2+} ground state $3d^{10}4f^7$ configuration are F^2=10.398 eV, F^4=6.486 eV, F^6=4.655 eV, and the spin orbit coupling parameter is 0.160 eV. For the final Eu^{2+} state ($3d^9 4f^8$) the Slater integral parameters (in eV) are F^2=11.031, F^4=6.896, F^6=4.954, G^1=4.921, G^3=2.882, G^5=1.990, and spin-orbit coupling parameter is 0.187 eV. Similarly, for Eu^{3+} the Slater integral parameters for the configuration of the initial state $3d^{10}4f^6$ are F^2=11.266 eV, F^4=7.071 eV, F^6=5.088 eV, and the spin-orbit coupling parameter is 0.175 eV. For the final state of Eu^{3+} ($3d^9 4f^7$) the Slater parameters are F^2=11.840, F^4= 7.442, F^6=5.358, G^1= 5.326, G^3=3.121, G^5=2.156 (all in eV), and spin-orbit coupling term is 0.202 eV. The values of the Slater parameters used in the calculations are consistent with those reported in the literature.[S2]

References:

S1. E. Stavitski, F. M. F. de Groot *Micron* 2010, **41**, 687

S2. B. T. Thole; G. van der Laan; J. C. Fuggle; G. A. Sawatzky; R. C. Karnatak; J.-M. Esteva *Phys. Rev. B* 1985, **32**, 5107

II. FIGURES

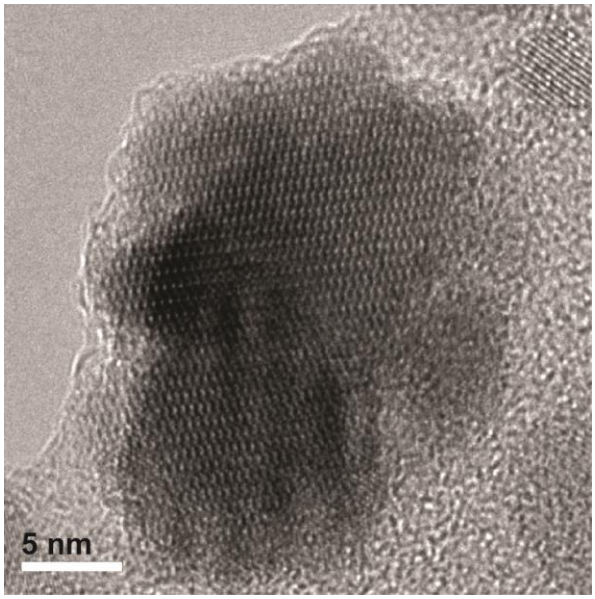

Fig. S1 Lattice-resolved TEM image of a single Eu-doped bcc-In_2O_3 "nanoflower" from the sample prepared at 300 °C with 15 % starting concentration of $EuCl_3$. Continuous lattice fringes indicate that the flower-like nanostructures were formed by the oriented attachment of colloidal NCs.

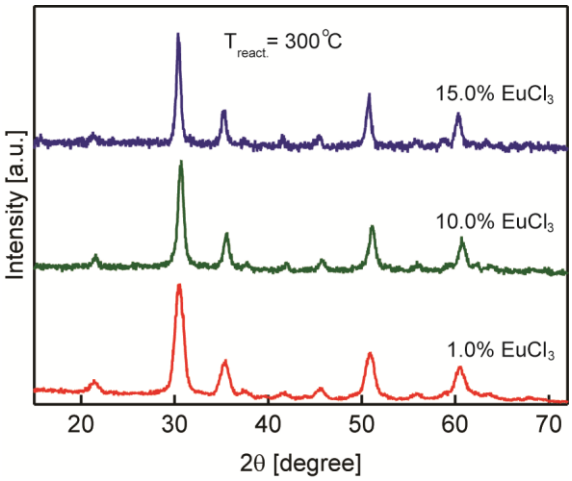

Fig. S2 XRD patterns of Eu-doped In_2O_3 NCs synthesized at 300 °C with different starting concentrations of $EuCl_3$ precursor, as indicated in the graph. All XRD patterns can be assigned to bixbyite-type crystal structure.

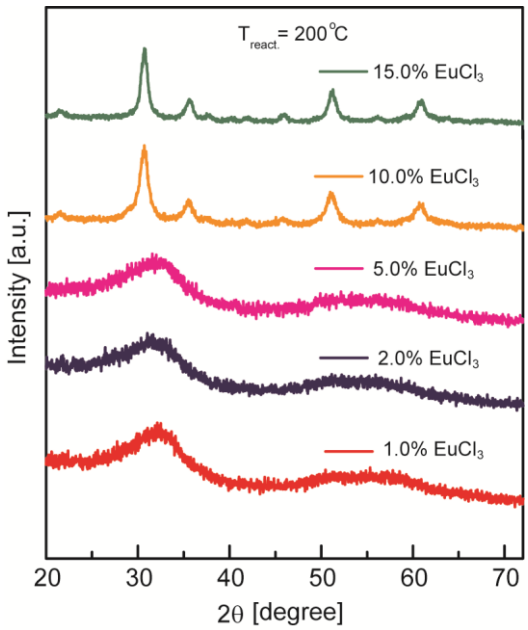

Fig. S3 XRD patterns of Eu-doped In_2O_3 NCs synthesized at 200 °C with different starting concentrations of $EuCl_3$ precursor, as indicated in the graph. For low starting concentrations of Eu precursor (below ca. 5%) the NCs have corundum-type crystal structure (rh-In_2O_3), while for higher Eu concentrations they adopt bixbyite structure (bcc-In_2O_3).

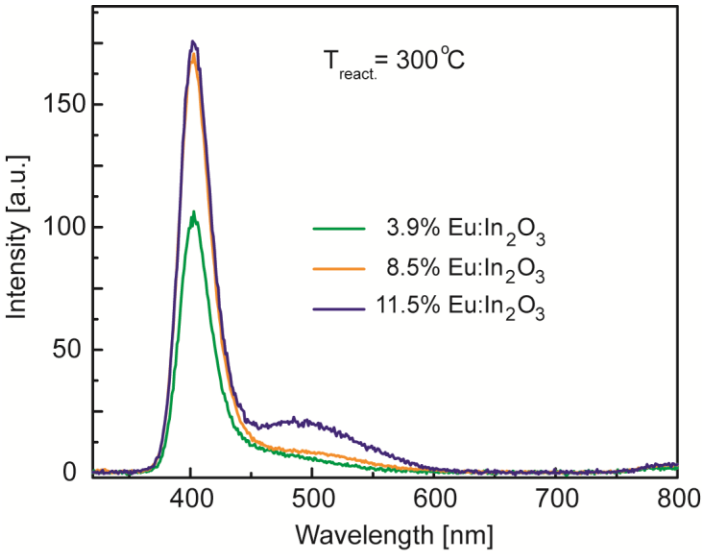

Fig. S4 PL spectra of Eu^{2+} in Eu-doped bcc-In_2O_3 NCs synthesized at 300 °C, having different doping concentrations (λ_{exc}= 300 nm). With increasing doping concentration the broad defect-based band centered at ca. 500 nm increases in intensity.

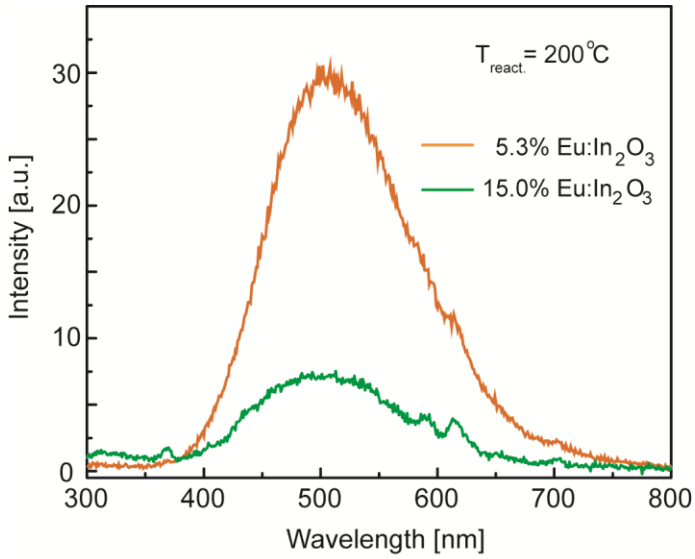

Fig. S5 PL spectra of Eu-doped In_2O_3 NCs synthesized at 200 °C upon excitation above the band gap energy. With increasing doping concentration the sharp Eu^{3+} transitions (580-700 nm) become more pronounced.

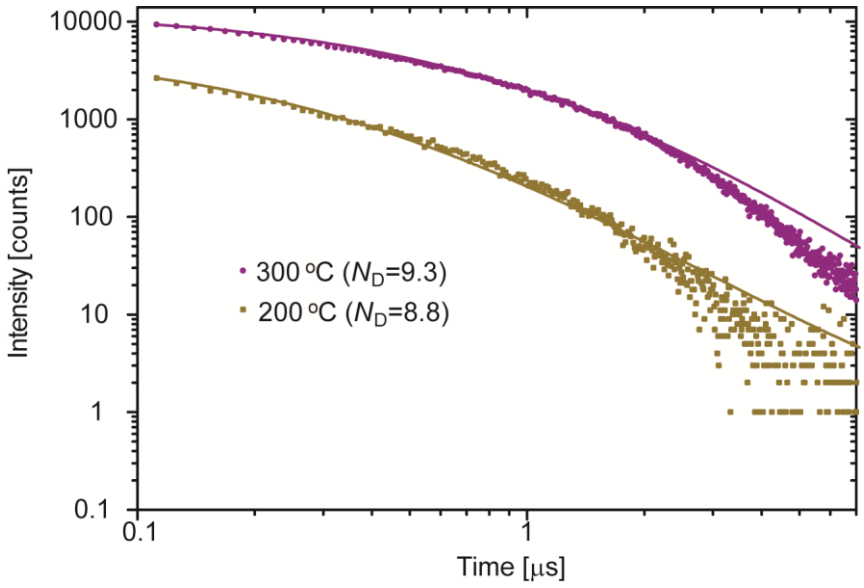

Fig. S6 (a) Time-resolved DAP PL decay of 10.5 % Eu-doped In_2O_3 NCs synthesized at 200 °C having an average size of ca. 7.5 nm (ocher dots), and 11.5 % Eu-doped In_2O_3 NCs synthesized at 300 °C having an average size of ca. 20.0 nm (purple dots). The solid lines represent the fits to the experimental data using DAP time decay model (see ref. 21). The number of donor defects N_D (oxygen vacancies) per NC, obtained as a fitting parameter, is shown in the graph. Although the absolute number of donor defects is similar the defect concentration is significantly higher in smaller NCs, consistent with our discussion in the main text. Since both samples have bcc-In_2O_3 crystal structure and comparable doping concentration, higher defect concentration (or smaller defect separation) arises from the lower synthesis temperature and higher surface-to-volume ratio of NCs synthesized at 200 °C.

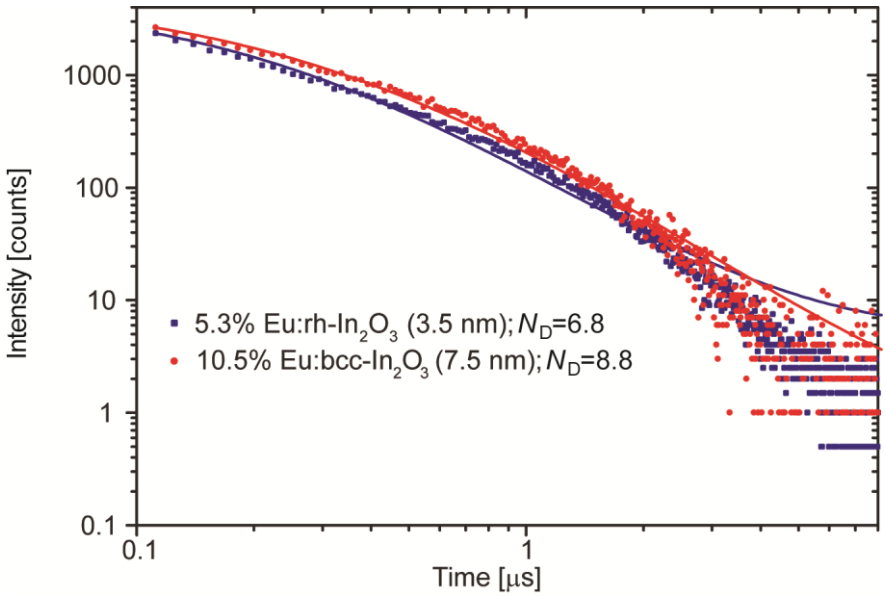

Fig. S7 Time-resolved DAP PL decay of 5.3 % Eu-doped rh-In_2O_3 NCs having an average size of ca. 3.5 nm (blue dots), and 10.5 % Eu-doped bcc-In_2O_3 NCs having an average size of ca. 7.5 nm (red dots) synthesized at 200 °C. The solid lines represent the fits to the experimental data using DAP time decay model. The number of donor defects N_D per NC, obtained as a fitting parameter, is shown in the graph. The defect concentration is more than 7 times higher in rh-In_2O_3 NCs. Higher propensity of defect formation in rh-In_2O_3 NCs is mostly associated with smaller NC size and higher surface-to-volume ratio.

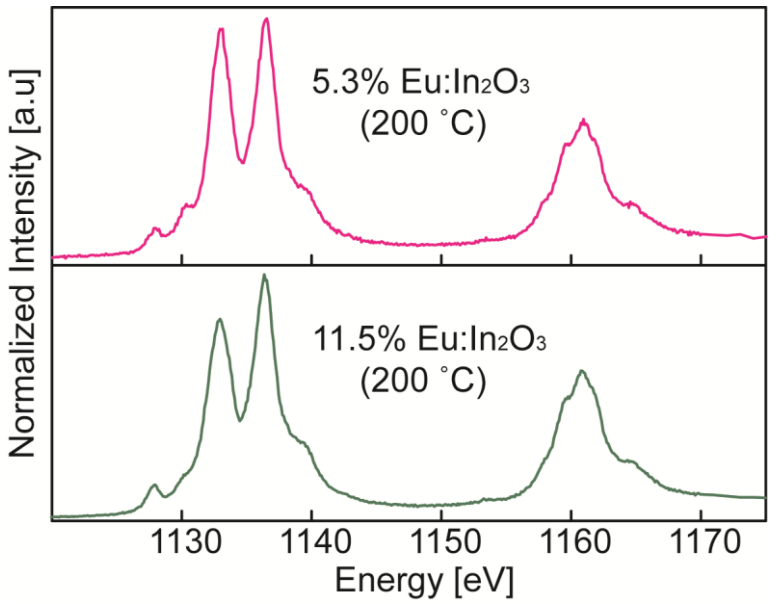

Fig. S8 Eu M-edge X-ray absorption spectra of 5.3 % (top) and 11.5 % (bottom) Eu-doped In_2O_3 NCs synthesized at 200 °C.

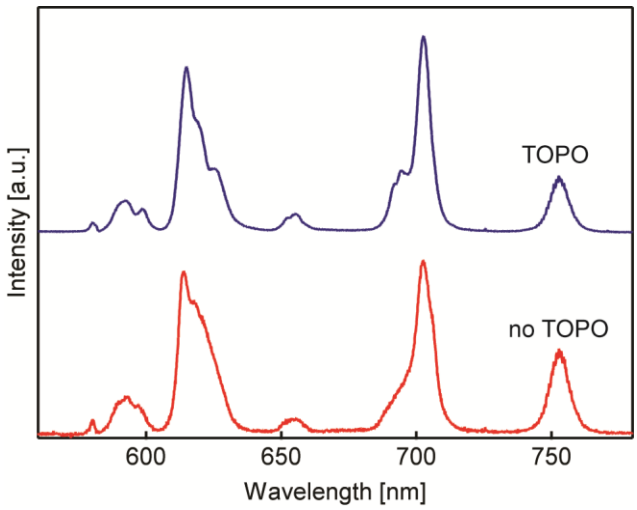

Fig. S9 High-resolution Eu^{3+} PL spectra of Eu-doped rh-In_2O_3 NCs synthesized at 200 °C before (bottom) and after (top) treatment with TOPO. Upon TOPO treatment the spectra become better resolved.

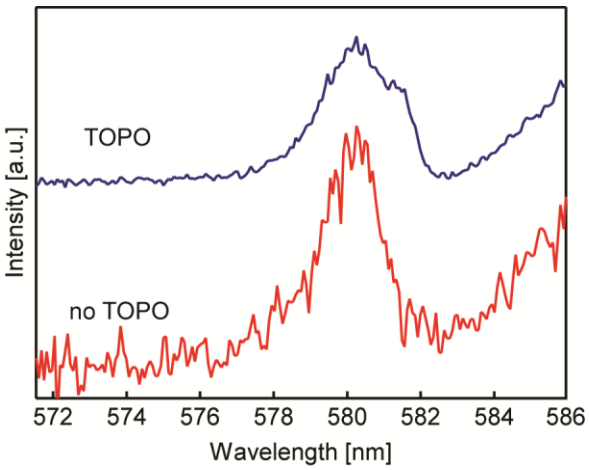

Fig. S10 High-resolution Eu^{3+} ($^5D_0 \rightarrow {}^7F_0$) PL spectra of samples in Fig. S9 before (bottom) and after (top) TOPO treatment. Without TOPO treatment only one broad structureless peak with the maximum at ca. 580.3 nm is observed, indicating a significant presence of Eu^{3+} in the NC surface region. Upon TOPO treatment this peak decreases in intensity revealing a narrow peak at ca. 581.5 nm, which is suggested to be due to internally incorporated Eu^{3+} (see main text for more details).